Journal of Applied Geophysics 116 (2015) 93–103

Contents lists available at ScienceDirect

Journal of Applied Geophysics

journal homepage: www.elsevier.com/locate/jappgeo

Effect of near-surface topography on high-frequency Rayleigh-wave propagation

Limin Wang [a,*], Yixian Xu [a,b], Jianghai Xia [a], Yinhe Luo [a,b]

[a] Hubei Subsurface Multi-scale Imaging Key Laboratory, Institute of Geophysics and Geomatics, China University of Geosciences, Wuhan, Hubei 430074, P.R. China
[b] State Key Laboratory of Geological Processes and Mineral Resources, China University of Geosciences, Wuhan, Hubei 430074, P.R. China

ARTICLE INFO

Article history:
Received 21 May 2014
Received in revised form 29 January 2015
Accepted 20 February 2015
Available online 28 February 2015

Keywords:
Topographic influence
High-frequency Rayleigh waves
Depressed topography
Uplifted topography

ABSTRACT

Rayleigh waves, which are formed due to interference of P- and Sv-waves near the free surface, propagate along the free surface and vanish exponentially in the vertical direction. Their propagation is strongly influenced by surface topography. Due to the high resolution and precision requirements of near-surface investigations, the high-frequency Rayleigh waves are usually used for near-surface structural detecting. Although there are some numerical studies on high-frequency Rayleigh-wave propagation on topographic free surface, detailed analysis of characters of high-frequency Rayleigh-wave propagation on topographic free surface remains untouched. Hence, research of propagation of Rayleigh waves on complex topographic surface becomes critical for Rayleigh-wave methods in near-surface applications. To study the propagation of high-frequency Rayleigh waves on topographic free surface, two main topographic models are designed in this study. One of the models contains a depressed topographic surface, and another contains an uplifted topographic surface. We numerically simulate the propagation of high-frequency Rayleigh waves on these two topographic surfaces by finite-difference method. Soon afterwards, we analyze the propagation character of high-frequency Rayleigh waves on such topographic models, and compare the variations on its energy and frequency before and after passing the topographic region. At last, we discuss the relationship between the variations and topographical steepness of each model. Our numerical results indicate that influence of depressed topography for high-frequency Rayleigh waves is more distinct than influence of uplifted topography. Rayleigh waves produce new scattering body waves during passing the depressed topography with reduction of amplitude and loss of high-frequency components. Moreover, the steeper the depressed topography is, the more energy of Rayleigh waves is lost. The uplifted topography with gentle slope produces similar influence as the depressed topography on propagation of high-frequency Rayleigh waves. When slopes are getting steep, however, the obstacle influence of the uplifted topography becomes weak. In addition, in the uplifted-topography case, part of Rayleigh-wave energy is absorbed by the uplifted terrain, which includes the trapped energy between the uplifted boundaries and the generation of scattering waves. Meanwhile, local topography strongly affects the character of Rayleigh-wave dispersion. Egregious error may be introduced, when pick Rayleigh-wave phase velocities on dispersion energy images for an MASW survey, if the local free-surface topography is ignored.

1. Introduction

Underneath shear (S)-wave velocity has gained popularity in engineering and environmental studies. Since it is directly proportional to shear modulus of underneath materials, it becomes a fundamental indicator of stiffness of earth material (Imai and Tonouchi, 1982). Evaluation of S-wave velocity profile has been one of the critical tasks in geotechnical engineering (e.g., Craig, 1992; Xia et al., 1999, 2002). At present, an S-wave velocity profile is often obtained by surface-wave method. For example, the Multichannel Analysis of Surface Wave (MASW) method (e.g., Xia et al., 1999, 2002) is one of the successful surface-wave methods. It is based on the dispersive nature of Rayleigh waves in vertically heterogeneous media and the horizontal layer assumption of earth model. The earth, however, is not composed of perfectly flat-layered medium. Clarifying propagation properties of Rayleigh wave in complex structure plays a critical role in understanding Earth structures (e.g., Zhao, 1991).

To our knowledge, surface-wave transmission is substantially affected by the irregular surface. The earliest reports of surface-wave propagation on topographic surface began in 1958. The studies include the transmission and reflection of Rayleigh waves at corners (deBremaecker, 1958), characters of reflection and transmission coefficient of angle topography by experiment studies (Knopoff and Gangi, 1960), and the theoretical formula of reflection and transmission at a corner (e.g., Hudson and Knopoff, 1964; Mal and Knopoff, 1965, 1966; Fujii et al., 1984). Snieder

* Corresponding author.
E-mail address: Liminwang_1983@126.com (L. Wang).

http://dx.doi.org/10.1016/j.jappgeo.2015.02.028
0926-9851/

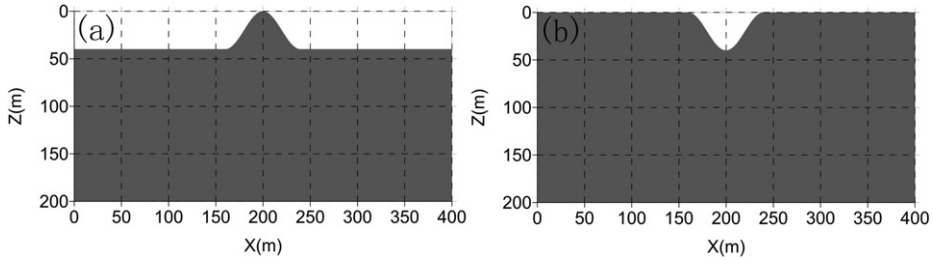

Fig. 1. Half-space earth model whose free surface contains (a) an uplifted topography, and (b) a depressed topography.

(1986) studied the effects of topography on three dimensional surface-wave scattering and conversions by the Born approximation method. In his study, the scattering of surface wave by topography was compared with the scattering of surface wave by a mountain root model. He also analyzed the interference effects between surface waves scattered by different parts of heterogeneity.

These previous theoretical results lead us to a considerable improvement in the explanation of real-world data and experiments. Analyzing the dispersion characters of Rayleigh waves on topographical surface, however, is too complicated. These studies are less general in either analytical method or numerical simulation. With the development of propagation theory of seismic waves and the progress of numerical simulation techniques, further studies of topographic influence on Rayleigh-wave propagation have been done. Numerical simulation techniques are important tools to remedy the weakness of analytical methods. They have been widely used in studying the problem of surface-wave propagation on complex geological structures. Fuyuki and Matsumoto (1980) simulated the scattering of Rayleigh waves on topographic free surface by the finite-difference method. Wong (1982) studied the frequency response of a canyon to Rayleigh waves. Kawase (1988) studied the time domain response of Rayleigh waves by the boundary element method. Afterwards, Sánchez-Sesma and Campillo (1991) discussed such response of more general topography.

Based on the boundary element method, Hévin et al. (1998) numerically simulated the propagation of Rayleigh waves across various surface cracks. From the simulation signals, the variations of spectral ratios between the transmitted and incident waves are studied as a function of the crack depth. Their study can be used to design an efficient procedure for the determination of crack depths. Zhang and Liu (2000) studied the problem of elastic wave diffraction on a semi-cylindrical pit-case topographical surface. They proved that Rayleigh-wave diffraction was stronger than P waves, when the wavelength of Rayleigh waves was shorter than the P waves. Cao et al. (2007) numerically simulated the propagation of Rayleigh waves across surface crack by the finite element method. At the same year, Nasseri-Moghaddam et al. (2007) numerically investigated the propagation of Rayleigh waves on solid space with cavity. Their numerical tests showed that the buried depth and the size of the cavity detected by the surface wave method were a function of Rayleigh-wave frequency spectrum. Zhou and Chen (2007) studied the effect of depressed topography on low-frequency (<2 Hz) Rayleigh waves stimulated by a near-surface explosive source. They pointed out that Rayleigh-wave energy and frequency response were changed when Rayleigh waves passed through the depressed topography.

In numerical modeling of high-frequency Rayleigh-wave propagation on topographic free surface, Zeng et al. (2012a) proposed an improved vacuum formulation to incorporate surface topography and internal discontinuity for finite-difference (FD) modeling of Rayleigh waves in the near surface. By their scheme, they numerically investigated the propagation of Rayleigh waves on topographic free surface (Zeng et al., 2012a), and the application of the MASW method in the presence of free-surface topography (Zeng et al., 2012b). Wang et al. (2012) developed an effective FD scheme to simulate Rayleigh-wave propagation in the topographical model, which incorporated Robertsson's 'staircase' method (Robertsson, 1996) and the acoustic/elastic interface approach (AEA approach) (Xu et al., 2007). Strong influence of topographic free surface on Rayleigh-wave propagation was demonstrated by numerical examples of three simple topographic models.

The previous numerical studies are all done either under the assumption of independent Rayleigh-wave source (Fuyuki and Matsumoto, 1980; Wong, 1982; Kawase, 1988; Sánchez-Sesma and Campillo, 1991), or under the assumption of low-frequency Rayleigh waves stimulated by explosive source (Zhou and Chen, 2007). However, due to the high resolution and precision requirements of near-surface investigations, the high-frequency Rayleigh waves are usually chosen for near-surface structural detecting. They are typically generated by a surface impact source, such as a sledgehammer hitting a steel plate. Research of propagation of high-frequency Rayleigh waves on topographic

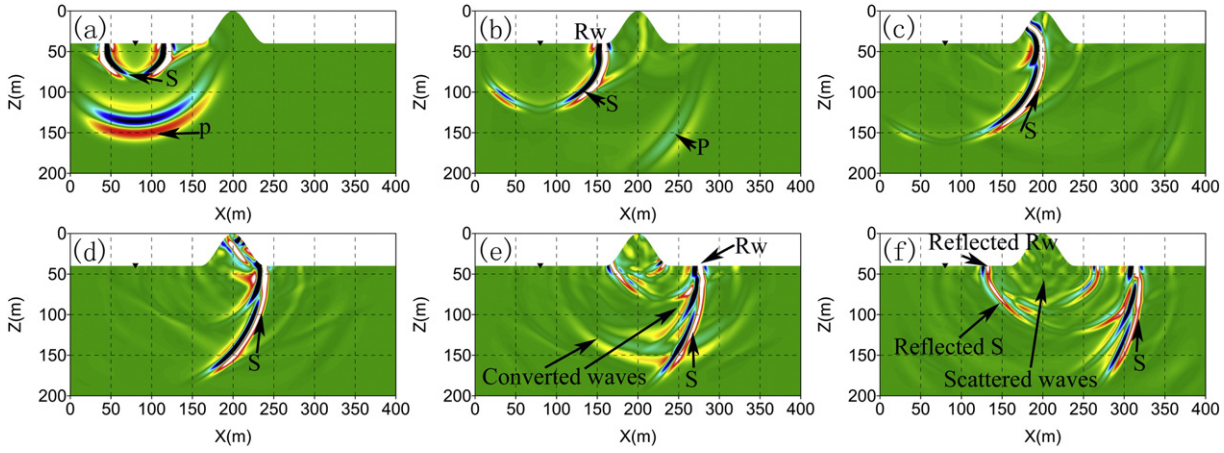

Fig. 2. Wave field snapshots of the vertical particle velocity for uplifted topographic model at time slice of (a) 0.1 s, (b) 0.2 s, (c) 0.3 s, (d) 0.4 s, (e) 0.5 s, and (f) 0.6 s. The solid triangles represent the location of the source.

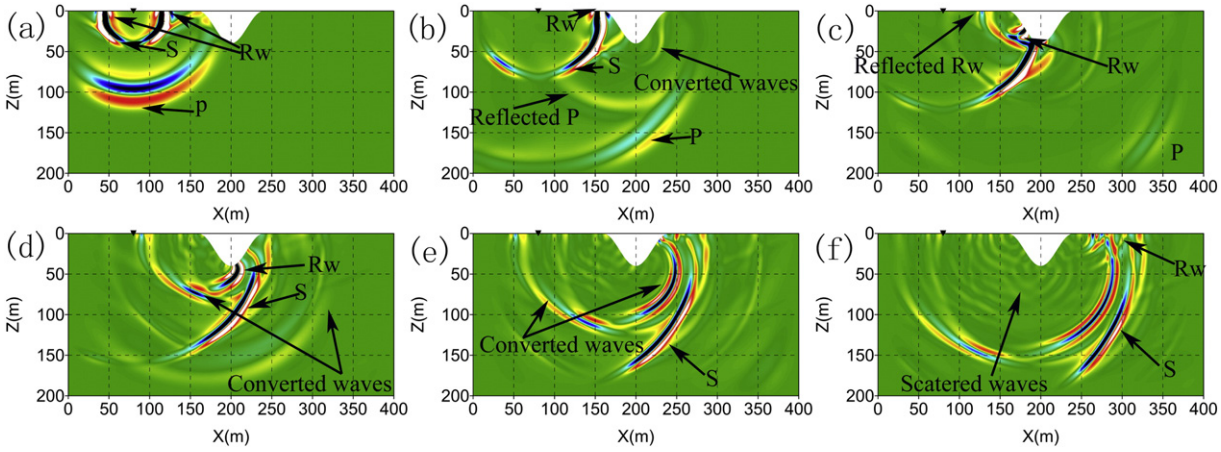

Fig. 3. Wave field snapshots of the vertical particle velocity for depressed topographic model at time slice of (a) 0.1 s, (b) 0.2 s, (c) 0.3 s, (d) 0.4 s, (e) 0.5 s, and (f) 0.6 s. The solid triangles represent the location of the source.

surface plays a critical role for surface-wave methods in near-surface applications. Though there are some numerical studies on high-frequency Rayleigh-wave propagation on topographic free surface (e.g., Nasseri-Moghaddam et al., 2007; Zeng et al., 2012a,b; Wang et al., 2012), detailed analysis of characters of high-frequency Rayleigh-wave propagation on topographic free surface remains untouched.

We configure a depressed and an uplifted topographic model to further study the propagation of high-frequency Rayleigh waves on topographic free surface. Propagation of high-frequency Rayleigh waves on these two topographic surfaces is numerically simulated by Wang's FD scheme (Wang et al, 2012). Based on the numerical simulations, we analyze the propagation character of high-frequency Rayleigh waves in such two typical topographic free surfaces, and discuss the variations of high-frequency Rayleigh waves in energy, frequency spectrum and amplitude response. Afterwards, we discuss the relationships between the variations and the topographical steepness of each model. Lastly, we analyze the influence of local topography on Rayleigh-wave dispersion characters.

2. Variation of propagation character of high-frequency Rayleigh waves on topography

Here, we design two homogeneous models with a canyon-case and a horst-case topographic free surface, respectively (Fig. 1). The width of the canyon and the horst is both 80 m. The maximum depth of the canyon and the maximum height of the horst are both 40 m. We numerically simulate the propagation of high-frequency Rayleigh waves by Wang's FD scheme (Wang et al., 2012). The models are 400 m × 200 m in size, and are discretized as 2000 × 1000 grid points. P- and S-wave velocities of each model are 1000 m/s and 400 m/s, respectively, and density is 2000 kg/m^3. No attenuation is considered in

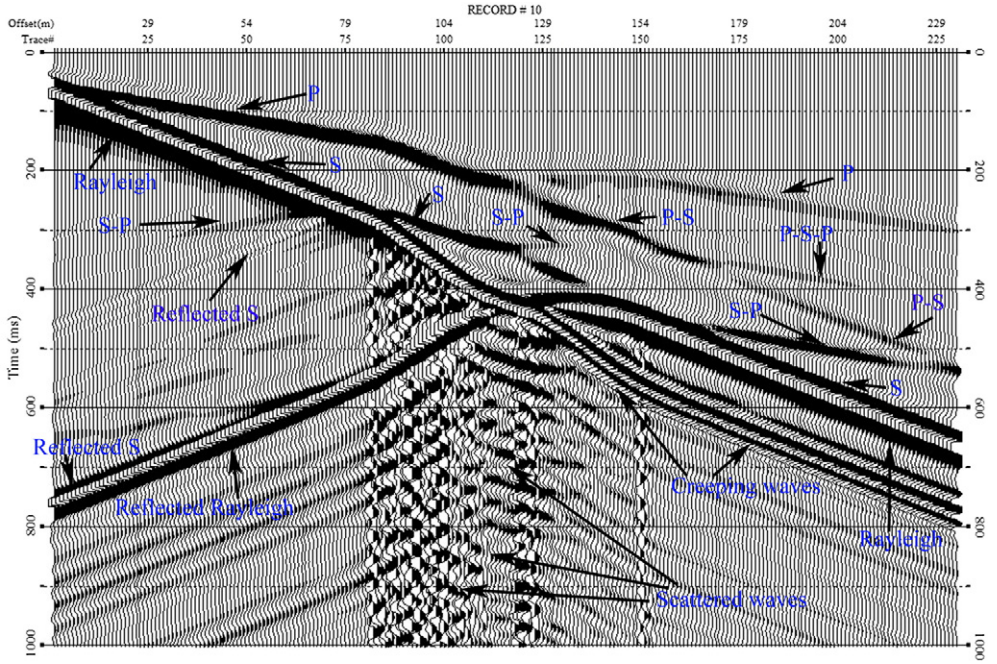

Fig. 4. The synthetic shot gather of vertical particle velocity generated for uplifted topographic model by Wang's FD code (Wang et al., 2012). The 230-channel receiver spread is located on the free surface across the topography, at the right side of the source. The nearest offset is 5.0 m, and the trace interval in the horizontal direction is a constant of 1.0 m. But the trace intervals measured along the free surface are different depending on the topography of its location. A large gain factor is applied to the display to enhance the visibility of the diffracted, the reflected and the converted events because the amplitudes of the diffractions, the reflections and the conversions from the uplifted topography corners are usually much lower than those of the incoming Rayleigh waves.

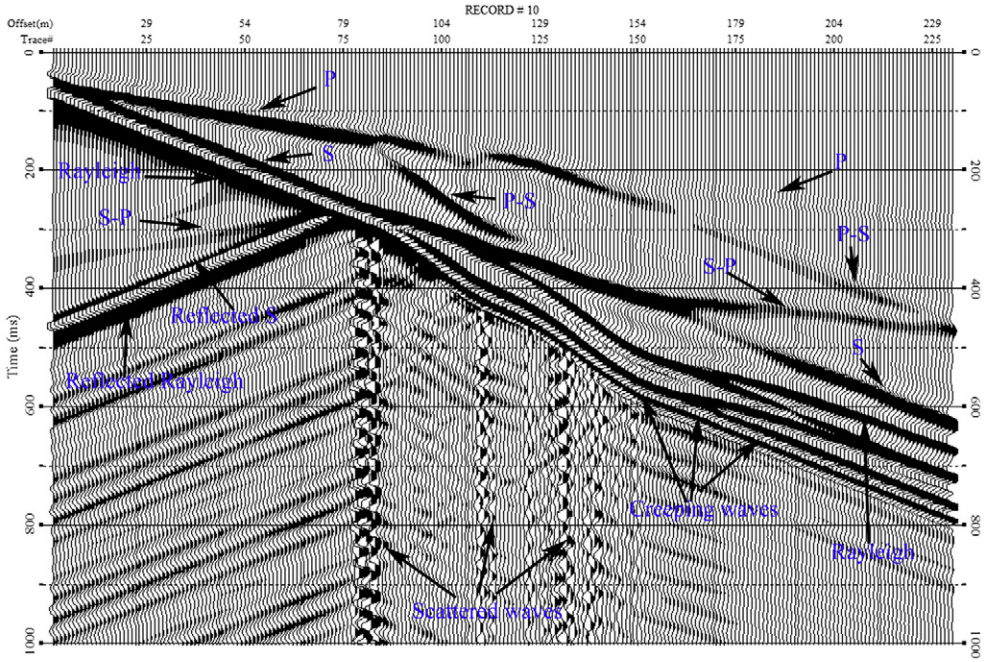

Fig. 5. The synthetic shot gather of vertical particle velocity generated for depressed topographic model by Wang's FD code (Wang et al., 2012). The 230-channel receiver spread is located on the free surface across the topography, at the right side of the source. The nearest offset is 5.0 m, and the trace interval in the horizontal direction is a constant of 1.0 m. But the trace intervals measured along the free surface are different depending on the topography of its location. A large gain factor is applied to the display to enhance the visibility of the diffracted, the reflected and the converted events because the amplitudes of the diffractions, the reflections and the conversions from the uplifted topography corners are usually much lower than those of the incoming Rayleigh waves.

the medium. The time marching step is 0.1 ms. The first derivative of Gaussian with 20 Hz peak frequency and 50 ms delay time is used as the source function of vertical point source (e.g., Mittet and Arntsen, 2000; Xu et al., 2007). The source is located at the horizontal free surface, 120 m away from the center of the topography.

Fig. 2 shows the snapshots of elastic-wave fields of the uplifted topographic model (Fig. 1a) at 0.1 s, 0.2 s, 0.3 s, 0.4 s, 0.5 s, and 0.6 s, respectively. These snapshots display the generation and transmission of body waves and high-frequency Rayleigh waves on the uplifted topographical free surface. Since the vertical point source is located on the flat free surface, both a P and an S wave are excited. Near the free surface, Rayleigh waves are generated from the constructive interference of P and S waves (Fig. 2a). P wave firstly passes the horst. When it arrives at the left, the top and the right corner of the horst, weak wave conversion and scattering occur. Then S wave and Rayleigh wave tread on the heels of P wave and pass through the horst. It shows that on the source-side corner (the left side of the horst), weak Rayleigh-wave reflection exist and propagate in opposite directions of the incoming Rayleigh waves (Fig. 2f). When S wave and Rayleigh waves reach to the top of the horst, abundant forward and backward scattered waves are generated (Fig. 2c and d). Meanwhile, new conversion P wave and new reflection or conversion Rayleigh waves generates (Fig. 2e). In addition, part of Rayleigh-wave energy is absorbed by the uplifted terrain (Fig. 2d and e), which includes the trapped energy between the uplifted boundaries and the generation of scattering waves (Fig. 2f).

For Rayleigh-wave propagation on the depressed topographic free surface, more complex features are shown on the snapshots (Fig. 3). Both a P, an S and a Rayleigh wave are generated (Fig. 3a). Throughout

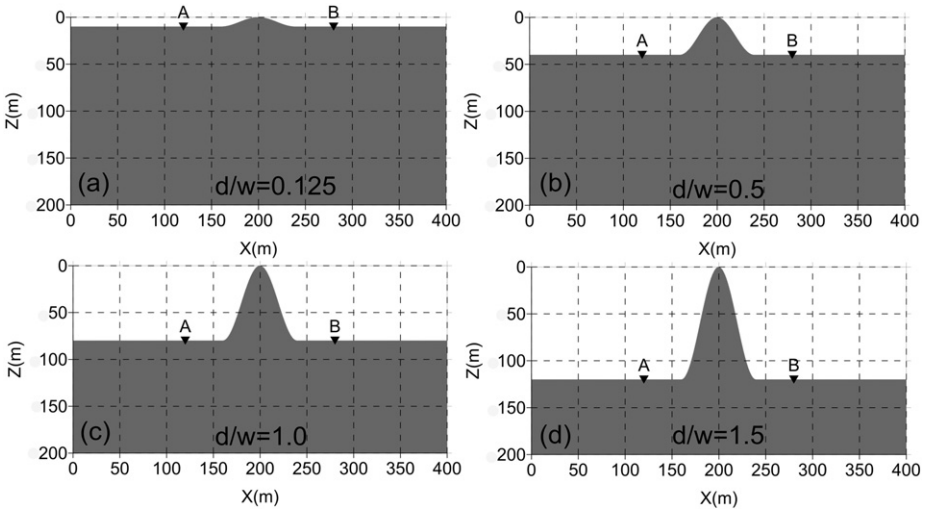

Fig. 6. The uplifted topographic models with different steepness. The horsts are of width 80 m and of maximum height changing from 10 m to 120 m with 10 m increment. Here, we only show the topographic models with steepness of (a) d/w = 0.125, (b) d/w = 0.5, (c) d/w = 1.0 and (d) d/w = 1.5, for example.

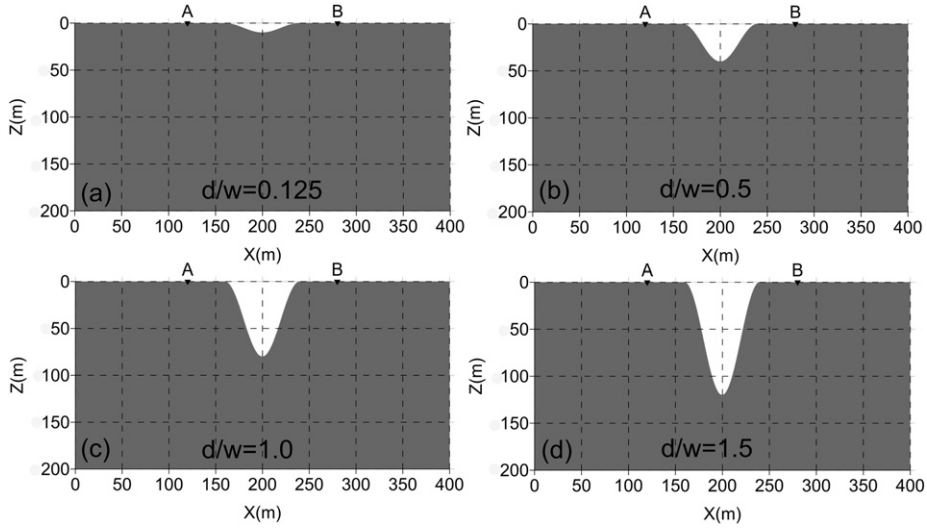

Fig. 7. The depressed topographic models with different steepness. The valleys are of width 80 m and of maximum depth changing from 10 m to 120 m with 10 m increment. Here, we only show the topographic models with steepness of (a) d/w = 0.125, (b) d/w = 0.5, (c) d/w = 1.0 and (d) d/w = 1.5, for example.

the whole process of seismic-wave propagation, P wave still firstly passes the valley. In the left corner (the near source-side corner) of the valley, P wave is reflected and converted to S wave and Rayleigh wave. Although the energy of the conversion Rayleigh wave is relatively weak, it still appears in snapshot (Fig. 3c). These reflections and conversions also appear in the right corner (the far source-side corner) of the valley (Fig. 3e and f). S wave and Rayleigh wave tread on the heels of P wave and pass through the valley. Strong reflection occurs in the left corner and propagates in opposite direction of the incoming Rayleigh waves. Meanwhile, S to P wave conversion occurs in the left corner (the near source-side corner) (Fig. 3c and d). Relatively weaker conversions appear in the right corner of the valley (the far source-side corner) (Fig. 3f). After passing the valley, abundant forward and backward scattered body waves and scattered Rayleigh waves are generated by the valley. Since their wave fronts are intercrossed, the whole wave field near the valley becomes very complex.

Meanwhile, complex reflections and conversions of seismic waves on topographic surface are shown on the corresponding synthetic seismograms (Figs. 4 and 5). Since the energy of Rayleigh waves dominate the whole wave fields, body waves are too weak to display clearly in the seismograms. Hence, to display the complicated reflection and conversion clearly, we perform trace equalization procedure and increase the data display gain in plotting the synthetic seismograms.

Clear P to S conversion occurs in the top of the horst (P–S in Fig. 4). In the right corner (far source side), however, this converted S wave (P–S) is converted back to P wave (P–S–P in Fig. 4). Weak S to P wave conversion occurs in the left corner of the horst (the near source-side corner). Then, part of S wave and Rayleigh wave directly penetrates through the horst and reaches to another side of the horst. Parts of S wave and Rayleigh waves, however, creep through the horst from the topographical free surface (creeping waves in Fig. 4). Strong reflection Rayleigh waves generate in the top of the horst. Hence, we can notice that the incoming Rayleigh wave and its reflection coexist and propagate in opposite directions on the source side (the left side of the peak of the horst). When S wave gets to the right corner of the horst, conversion appears again. New S to P conversion wave is generated. As previously described, parts of Rayleigh-wave energy is trapped between the boundaries of the horst and is multi-reflected by the boundaries. Hence, in the uplifted terrain, abundant of scattering waves is generated in the uplifted terrain. These scattering (or diffraction) wave components consist mostly of Rayleigh waves, at some distance away from the horst (Bouchon et al., 1996).

Synthetic seismogram of the depressed topographical model (Fig. 1b) is shown in Fig. 5. Different to seismogram of the uplifted topographical model, the strong conversion of P wave to S wave appears in the left corner of the valley (the near source-side corner). This converted S wave (P–S wave in Fig. 5) connects with the incoming S wave on the bottom of the valley. On the right corner (the far source side) of the valley, clear conversion of S wave to P wave (S–P wave in Fig. 5) appears in. Meanwhile, weak conversion of P wave to S wave occurs in this corner. S wave and Rayleigh wave are strongly reflected on the left corner of the valley. This strong reflection leads to a shadow zone in the right side (far source side) of the valley. Only a few parts of body-waves and Rayleigh-waves energy can creep through the valley. Moreover, the wave scattering appears in the left, right and bottom corner of the valley. Among these scattering waves, the strongest scattering waves are generated on the left corner.

In summary, the incoming seismic waves are interacted with the irregular topography and produce new scattering and conversion waves. Numerical comparison results indicate that the influence of the

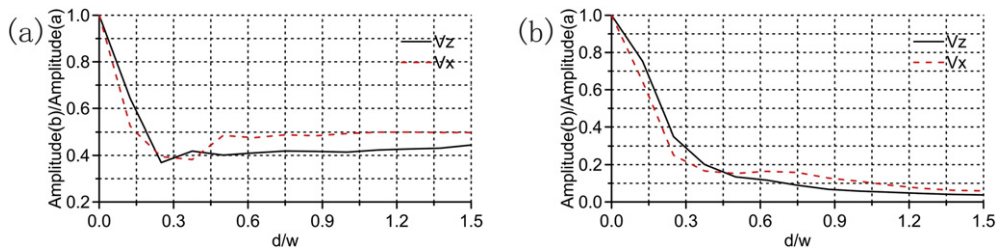

Fig. 8. Energy ratio of Rayleigh waves at point A and point B for (a) the uplifted topographic models, and (b) the depressed topographic models. The solid black line represents the energy ratio curve for components of vertical particle velocity (Vz), and the dashed red line represents the energy ration curve for components of horizontal particle velocity (Vx).

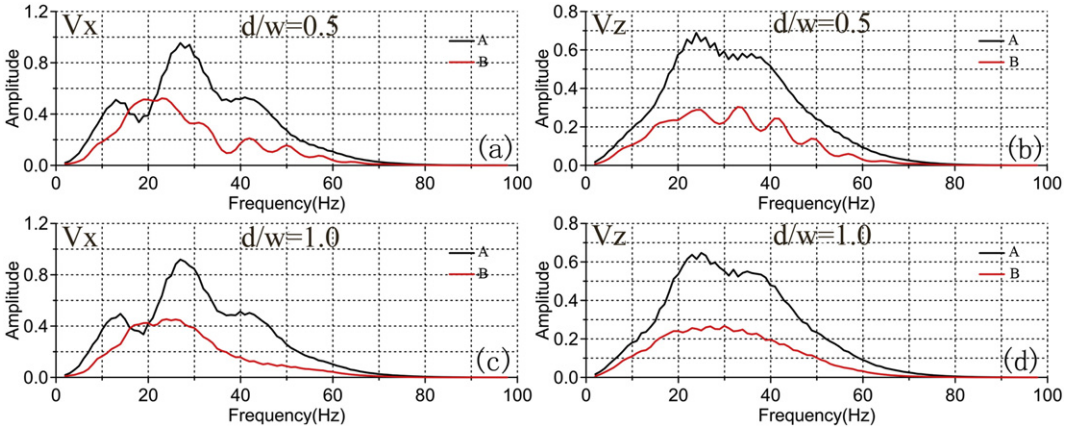

Fig. 9. The comparisons of Rayleigh-wave frequency spectrum between seismograms of horizontal particle velocity at points A and B of uplifted topographic models with steepness of (a) d/w = 0.5, and (c) d/w = 1.0, and seismograms of vertical particle velocity at points A and B of uplifted topographic models with steepness of (b) d/w = 0.5, and (d) d/w = 1.0. The solid black line denotes frequency spectra of seismogram at point A. The solid red line denotes frequency spectra of seismogram at point B. Vx and Vz denote horizontal particle velocity and vertical particle velocity, respectively.

depressed topography for high-frequency Rayleigh waves is more distinct than the influence of the uplifted topography. For an uplifted topographic model, part of Rayleigh wave energy is trapped between the boundaries of the horst. Meanwhile, the trapped Rayleigh waves will be multi-reflected by the boundaries. This phenomenon reveals a fact from a certain extent. On earthquake, the buildings on the top of a mountain are often damaged worse than the buildings on plain areas. It is valuable for earthquake engineering, although it is out of scope of our research.

3. The influence of topographical steepness on propagation of high-frequency Rayleigh waves

Usually, a surface impact source is chosen to generate the high-frequency Rayleigh waves in applications of Rayleigh-wave methods in near surface, for example the MASW method (e.g., Xia et al., 2002). Since the Rayleigh-wave energy dominates the whole wave field, it is unnecessary to mute the body waves before generating the dispersion curve. Moreover, Rayleigh waves are dominant in our simulating wave field. Hence, we can analyze the changes of whole wave filed to study the influence of surface topography on propagation of high-frequency Rayleigh waves. Due to the topography of the earth surface formed by weathering, deformation, etc., receivers are usually not located in the same elevation in MASW tests. As a consequence, the energy concentration on the dispersion energy images is usually distorted. In this case, it is difficult to pick an accurate dispersion curve by the conventional energy tracing method. Huge errors can be introduced to the subsequent inversion procedures of MASW test. Hence, the analyzing results will be very helpful in guiding the applications of the MASW method in near surface.

To discuss the influence of topographical steepness on propagation of Rayleigh waves, we study the uplifted and the depressed models with fixed width of w = 80 m. Their maximum heights (or depths) (d) are increase from 10 m to 120 m with increments of 10 m. Then, the topographical steepness is described by the ratio of d/w. The elastic parameters are the same as the previous models. The shape of the uplifted (or depressed) topography is controlled by a sine function (or cosine function). Here we only choose the topographic models with steepness of d/w = 0.125, d/w = 0.5, d/w = 1.0, and d/w = 1.5, respectively, for example (Figs. 6 and 7).

3.1. The changes of energy

In discussing the influence of topographical steepness on propagation of Rayleigh waves, the energy variation of Rayleigh waves is firstly considered. Seismograms of two points (the inverted triangle marked

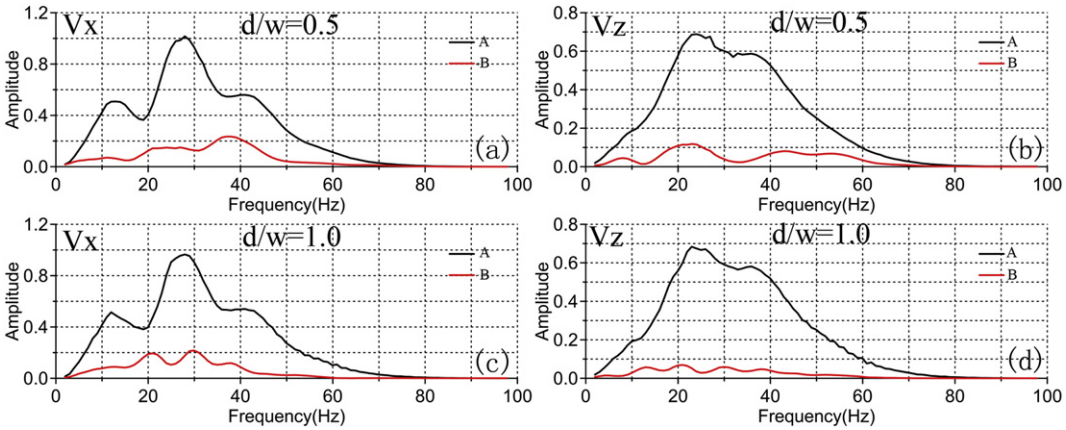

Fig. 10. The comparisons of Rayleigh-wave frequency spectrum between seismograms of horizontal particle velocity at points A and B of depressed topographic models with steepness of (a) d/w = 0.5, and (c) d/w = 1.0, and seismograms of vertical particle velocity at points A and B of depressed topographic models with steepness of (b) d/w = 0.5, and (d) d/w = 1.0. The solid black line denotes frequency spectra of seismogram at point A. The solid red line denotes frequency spectra of seismogram at point B. Vx and Vz denote horizontal particle velocity and vertical particle velocity, respectively.

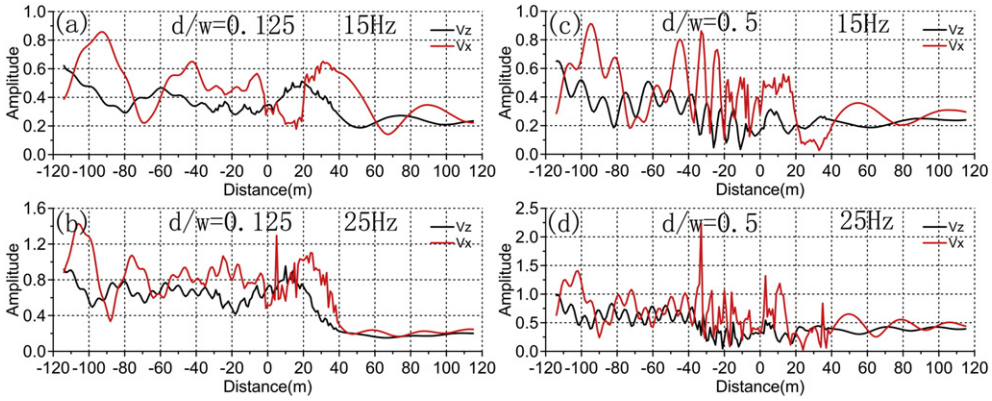

Fig. 11. The amplitude versus offset response of different frequency components for the uplifted topographic models with steepness of d/w = 0.125 ((a) 15 Hz, (b) 25 Hz), and d/w = 0.5 ((c) 15 Hz, (d) 25 Hz). The solid black lines denote the amplitude response of vertical particle velocity. The solid red lines denote the amplitude spectrum of horizontal particle velocity. The horizontal axis shows the distance between the positions of seismograms used in calculation and the central of the horst. The negative distances denote that the seismograms used in calculation are received at the source side. The positive distances denote that the seismograms used in calculation are received at the far source side.

with A and B in Figs. 6 and 7) of the topographic models are chosen. Point A is located at the left side (the near source side) of the horst (or canyon), 80 m away from the center of the horst (or canyon). Point B is located at the right side (the far source side) of the horst (or canyon), also 80 m away from the center of the horst (or canyon). In these two places, Rayleigh waves and the scattering waves are stable. No new conversion and scattering waves are generated. Theoretically, we can use the amplitude ratio of seismograms at points A and B as the energy ratio of points A and B (Fig. 8). In the images, the horizontal axis is the steepness of the topography (d/w), which ranges from 0 to 1.5. The vertical axis is the energy ratio. The solid black lines denote the energy ratio of seismogram of vertical particle velocity, and the dashed red lines denote the energy ratio of seismogram of horizontal particle velocity.

With the steepness of d/w increasing, less and less of Rayleigh-wave energy is left in the far source side of the uplifted topography (Fig. 8a). This phenomenon reveals the obstacle influence of horst-case topography on propagation of high-frequency Rayleigh waves. When topographic slopes are getting steep (e.g., d/w > 0.5), however, there is less variation in the energy ratio of seismograms at points A and B. This indicates that when the steepness of the horst increases to a certain value, part of Rayleigh wave energy directly penetrates from one side to another. Then, the energy ratio of points A and B keeps to a value of approximate 40% for vertical particle velocity and 50% for horizontal particle velocity. These ratios depend on the fixed width of topography, the source parameters and the elastic parameters which we configure in the numerical simulation. This study also indicates that the topography impacts propagation of seismic waves when the seismic wavelength is comparable to the horizontal size of topographic features.

Similar to the uplifted topography, with d/w increasing, Rayleigh waves have less energy left after passing through the canyons (Fig. 8b). Model with steepness of d/w = 1.5 which is the steepest canyon, shows that less than 10% energy is left after passing such depressed topography for both the horizontal and the vertical components. It means that the steeper the depressed topography the more energy of Rayleigh waves is lost. By comparison, more Rayleigh-wave energy is lost, in the depressed topographic case. In the far source side of the canyon, a shadow zone exists. Meanwhile, the more steeper the canyon gives rise to a wider range of the shadow zone.

3.2. The changes of frequency spectrum

In order to analyze the variation of Rayleigh-wave frequency spectrum in the process of wave transmission on the topographical free-surface, we calculate the frequency spectrum of seismograms at points A and B. Here, we choose the spectrums of seismograms of the models with topographical steepness of d/w = 0.5 and d/w = 1.0 for example.

When the free surface of the half-space model is horizontal, the shapes of the frequency spectrums of seismograms in different receivers

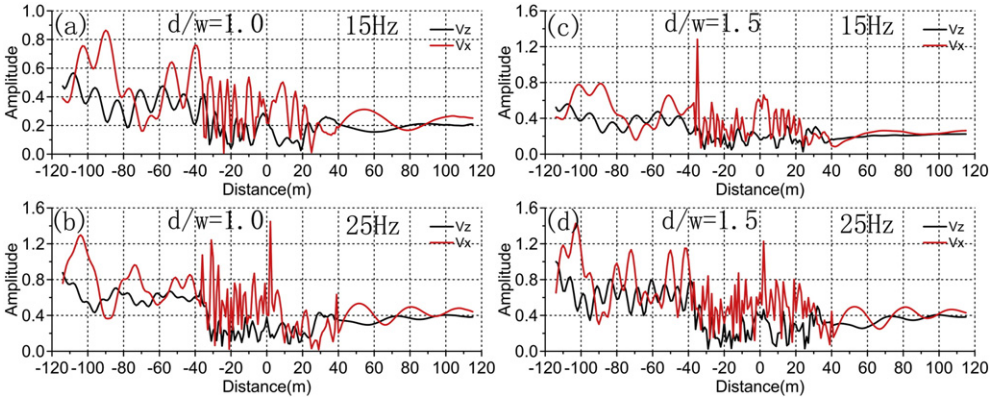

Fig. 12. The amplitude versus offset response of different frequency components for uplifted topography with steepness of d/w = 1.0 ((a) 15 Hz, (b) 25 Hz), and d/w = 1.5 ((c) 15 Hz, (d) 25 Hz). The solid black lines denote the amplitude response of vertical particle velocity. The solid red lines denote the amplitude spectrum of horizontal particle velocity. The horizontal axis shows the distance between the positions of seismograms used in calculation and the central of the horst. The negative distances denote that the seismograms used in calculation are received at the source side. The positive distances denote that the seismograms used in calculation are received at the far source side.

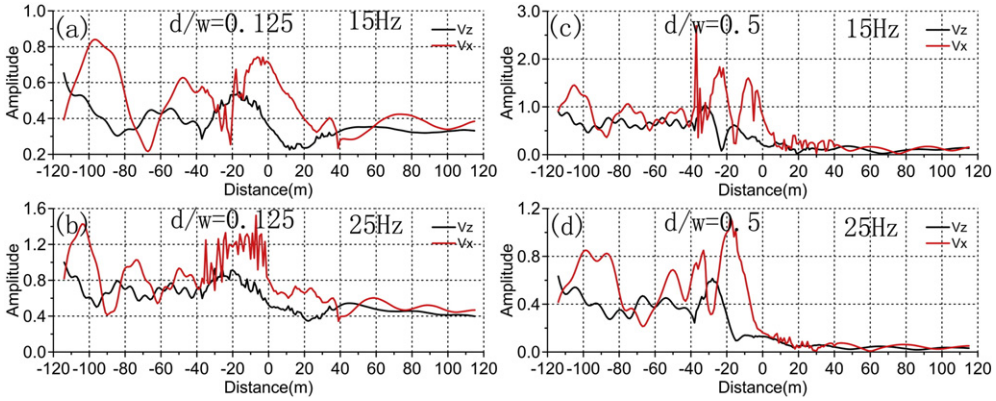

Fig. 13. The amplitude versus offset response of different frequency components for depressed topography with steepness of d/w = 0.125 ((a) 15 Hz, (b) 25 Hz), and d/w = 0.5 ((c) 15 Hz, (d) 25 Hz). The solid black lines denote the amplitude response of vertical particle velocity. The solid red lines denote the amplitude spectrum of horizontal particle velocity. The horizontal axis shows the distance between the positions of seismograms used in calculation and the central of the horst. The negative distances denote that the seismograms used in calculation are received at the source side. The positive distances denote that the seismograms used in calculation are received at the far source side.

are similar. They are controlled by the source function type. However, since the uplifted topographic free surface is introduced to the models, the shape of the corresponding frequency spectrum is changed (Fig. 9). The first change is the descending of the spectrum amplitude at the far source side (at point B). Since no attenuation is considered in the medium, the normal descending of the amplitude of the seismogram is only connected with the normal spherical diffusion. However, the descending of the amplitude of frequency spectrum at the far source side is far beyond the descending range of the normal spherical diffusion. The second change is that more peaks appear in the frequency spectrum. When wave propagate through the uplifted topography, wave reflection and conversion occur. The interference between the reflection/conversion waves and the incoming waves results in complex of the whole wave fields. Some frequency contents are decayed because of antiphase superposition. On the contrary, some frequency contents are amplified because of in-phase superposition. These may be the reason of more peaks appearing in the frequency spectrum. Moreover, with increasing horst steepness, the peaks move more obviously to low frequency band. This reveals that the high frequency contents are more easily reduced, when Rayleigh waves pass through the topographic surface.

Similar variation characters appear in the frequency spectrums of seismograms of the depressed topographical models (Fig. 10). Compare with the uplifted case, the peaks move more obviously to low frequency band with the increasing of valley steepness. More energy is lost with the increasing of valley steepness. This indicates that the depressed topography blocks more Rayleigh-wave energy than the uplifted topography, when Rayleigh waves propagate on the topographic free surface. More high-frequency contents are reduced on the depressed topography than on the uplifted topography. Meanwhile, for the depressed case, there are more wave reflection and wave conversion.

In conclusions, two reasons may give rise to the changes of the frequency spectrum. First, high-frequency contents decay more easily in propagation, especially in the topographical model. This leads the peak amplitude of the frequency spectrum to move from high frequency band to low frequency band. Second, wave conversion and scattering occur in the topographical model. The conversion, scattering and incoming wave interfere with each other. These interferences result in the complication of the wave fields. Meanwhile, parts of wave contents decay, and parts of wave contents are strengthened. These leads to more peaks that appear in the frequency spectrum. This phenomenon is more obvious for the depressed topography than for the uplifted topography. The comparisons further reveal the fact that the influence of the depressed topography is more distinct than the influence of the uplifted topography on propagation of high-frequency Rayleigh waves.

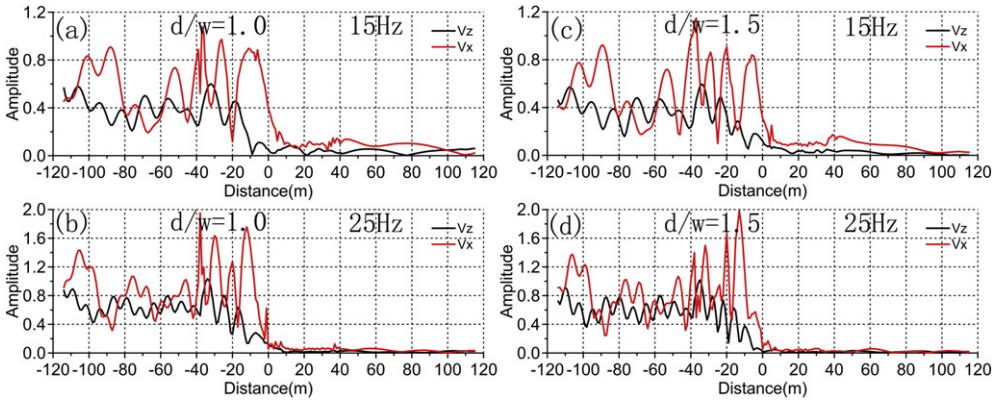

Fig. 14. The amplitude versus offset response of different frequency components for depressed topography with steepness of d/w = 1.0 ((a) 15 Hz, (b) 25 Hz), and d/w = 1.5 ((c) 15 Hz, (d) 25 Hz). The solid black lines denote the amplitude response of vertical particle velocity. The solid red lines denote the amplitude spectrum of horizontal particle velocity. The horizontal axis shows the distance between the positions of seismograms used in calculation and the central of the horst. The negative distances denote that the seismograms used in calculation are received at the source side. The positive distances denote that the seismograms used in calculation are received at the far source side.

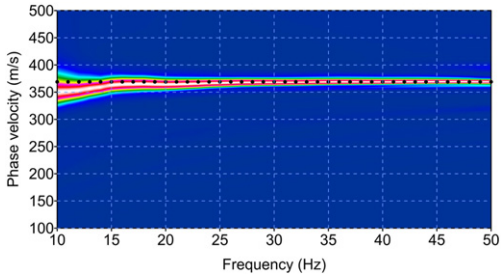

Fig. 15. The dispersion energy images of Rayleigh waves in the elastic homogeneous half-space model. The energy image is generated by the HRLRT method (Luo et al., 2008). The black dots denote the analytical dispersion curves of Rayleigh waves in elastic homogeneous half-space model, which are calculated by Knopoff method (Schwab and Knopoff, 1972).

3.3. Amplitude response versus offset

Images of amplitude response versus offset of Rayleigh waves in the topographic models are shown in Figs. 11–14. Here we only choose the results of topographic models with steepness of d/w = 0.125, d/w = 0.5, d/w = 1.0, and d/w = 1.5, for example. Frequency components of particle velocity with frequency of 15 Hz and 25 Hz are shown in the images, which represent the low-frequency components and the relatively high-frequency components, respectively. Both the response of the horizontal particle velocity (Vx, the red lines) and the vertical particle velocity (Vz, the black lines) are calculated. In the images, the horizontal axes represent the relative distances between the receivers and the center of the topographic area. The negative distances represent that the receivers are located on the near source side of the topographic area. The correspondent positive distances represent that the receivers are located on the far source side of the topographic area. The vertical axes represent the normalized amplitude of the frequency components of particle velocity.

For the uplifted topography (Figs. 11 and 12), Rayleigh-wave amplitude is perceptibly reduced after passing the horst, especially for the high-frequency component (Figs. 11b, d, 12b and d). When d/w is 0.125, the variation in amplitude response of the low-frequency component is smooth. However, for their corresponding high-frequency components, the amplitude variations are distinguishable in the amplitude-response images (Fig. 11b). When the slopes of the horst are getting steep (e.g., d/w > 0.5), there are less and less variation in amplitude response of each frequency components after passing through the horsts. Both the amplitude of the low-frequency components and the high-frequency components are distinguishably reduced after Rayleigh waves passing through the uplifted terrain. However, there is still nearly 40–50% Rayleigh-wave energy left in the far source side of the uplifted terrain.

Since the depressed topography leads to huge physical differences in horizontal direction of the Rayleigh-wave propagation path, strong reflections, conversions and refractions of Rayleigh waves occur in the near-source-side corner of the depressed topography. These produce distinguishable variations in the amplitude response versus offset of Rayleigh waves of the depressed topographic models (Figs. 13 and 14). Rayleigh-wave amplitude is dramatically reduced after they pass through the depressed topographic terrain. There are three similar variation characters for the amplitude response of Rayleigh waves in the depressed topography, although the slopes of the canyon are different. First, Rayleigh-wave amplitude reduces obviously in the process of wave propagation on the depressed topographical free surface. Second, the amplitude of Rayleigh waves received on the near source side is much larger than that on the far source side. Third, there is more energy left for low frequency components on the far source side of the canyon, while less for high frequency components.

3.4. The changes of Rayleigh-wave dispersion

Traditionally, Rayleigh waves are not dispersive in homogeneous half space. However, when the free surface of the half-space model is aligned with topography, are the Rayleigh waves still not dispersive? To study the effect of topographic surface on Rayleigh-wave dispersion, we numerically simulate the propagation of Rayleigh waves on elastic homogeneous half space and the previously described elastic half-space models with topographical free surface. The elastic parameters of the homogeneous half-space model are same with the previously described topographical models. The corresponding dispersion energy images (Fig. 15) are generated by the high-resolution linear Radon transform (HRLRT) method (Luo et al., 2008). The HRLRT method is an effective method to generate high-quality dispersion energy curve of surface wave in MASW technique. In the energy image, the peak amplitude trends of the dispersion energy match well with the analytical dispersion curve of Rayleigh waves in elastic homogenous half space (black

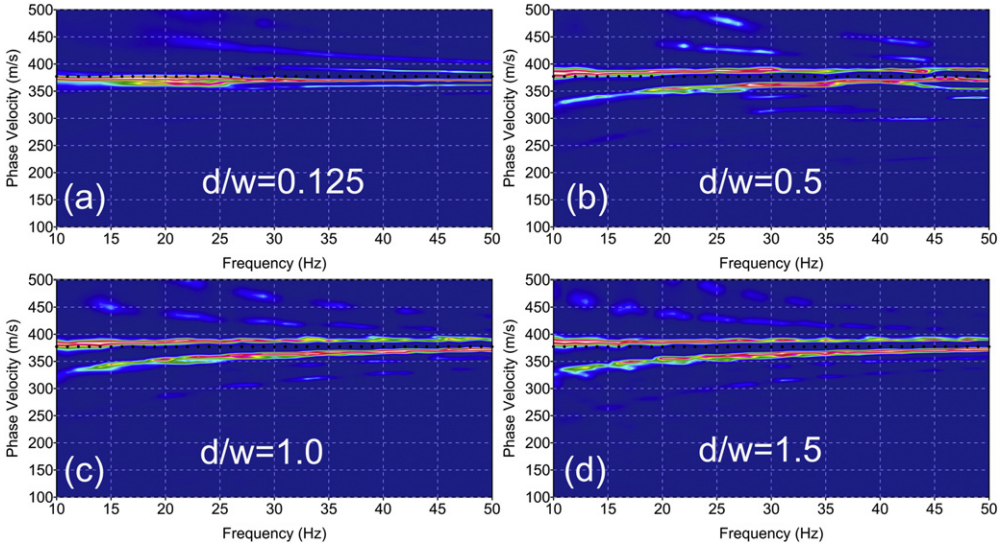

Fig. 16. The dispersion energy images of Rayleigh waves in elastic half-space model with uplifted topographic free surface. The energy images are generated by HRLRT method (Luo et al., 2008). The black dots denote the analytical dispersion curves of Rayleigh waves in elastic homogeneous half-space model, which are calculated by the Knopoff method (Schwab and Knopoff, 1972). Figures (a) to (d) are the dispersion energy images of Rayleigh waves in uplifted topographic model with the steepness of d/w = 0.125, d/w = 0.5, d/w = 1.0, and d/w = 1.5, respectively.

dots in Fig. 15). The analytical solutions are calculated by the Knopoff method (Schwab and Knopoff, 1972). This result demonstrates that Rayleigh waves are not dispersive in elastic homogeneous half-space model.

For the previously described elastic half-space model with uplifted topography, however, the energy concentration is distorted on the calculated dispersion images. Fig. 16a–d illustrates the corresponding dispersion images when steepness (d/w) of the horst is 0.125, 0.5, 1.0, and 1.5, respectively. When the slope is gentle (e.g., d/w = 0.125), the amplitude trends of dispersion energy image match with theoretical dispersion curves (indicated by the dots) with minor difference (Fig. 16a). With the increasing of steepness of the horst, the energy concentration is distorted and poses a few false "dispersion" (Fig. 16b–d). More than two energy concentration treads appear in the dispersion energy images. This may lead to an interpretation that Rayleigh-wave phase velocity changes with frequency in these models. Meanwhile, it is too hard to pick a right Rayleigh-wave phase velocity curve in these dispersion energy images. As discussed in previous parts, when steepness of the horst increases to a certain value (d/w = 0.5), parts of Rayleigh-wave energy penetrate directly from the near-source side to the far-source side. Hence, when steepness of the horst increases to a certain value (d/w = 0.5), there are less and less variations in dispersion energy images with increasing of the topography steepness.

Similar to the dispersion images of the uplifted models, the energy concentration of the dispersion energy images of the depressed models match with the theoretical dispersion curves with minor difference, when the slope is gentle (Fig. 17a). With the increasing of steepness, however, the energy concentration of dispersion energy images is distorted, especially in low frequency band. Compare to the dispersion energy images of the uplifted topography models, distinguishable distortions of energy concentration of dispersion energy images appear in the low frequency band (Fig. 17c–d). This may lead to a trouble in picking the right phase velocity of Rayleigh waves, and an interpretation that Rayleigh-wave phase velocity varies with the frequency. As a consequence, in this case, the earth model may not be correctly inverted from the picked dispersion curves due to the errors associated with the dispersion energy images.

In summary, free-surface topography strongly affects the Rayleigh-wave dispersion characters. Egregious error may be introduced in picking the dispersion curve by the conventional energy tracing method, when the receivers are not located in a same elevation and no static correction is applied for an MASW survey. The reason for surface topography distorting the dispersion energy of Rayleigh waves may be the strong reflection, conversion and scattering of Rayleigh waves on topographical surface. This energy distortion leads to an explanation that Rayleigh wave phase velocity is changed by surface topography. This has been firstly pointed out by Snieder (1986). Now, our numerical examples further prove this statement.

4. Conclusions

We configure two typical kinds of topographical half-space models to study the influence of local topography on propagation of high-frequency Rayleigh waves. Numerical simulations demonstrate that the steeper the depressed topography, the more Rayleigh waves are lost. Furthermore, the steeper the depressed topography, the wider the shadow zones in the far source side of the depressed topography. Not only Rayleigh-wave energy is changed, but also wave conversions occur and the frequency responses are changed, in the process of Rayleigh waves propagating on the topographical free surface. With the increasing of steepness of topography, the amplitude peak moves to low frequency band obviously in the frequency spectrum. Similar depressed topography takes similar influence on Rayleigh waves. Results of the uplifted topography with gentle slopes (e.g., d/w < 0.5) display that it produces the similar influence as the depressed topography on propagation of high-frequency Rayleigh waves. When slopes are getting steep (e.g., d/w > 0.5), however, the obstacle influence of the uplifted topography becomes weak. Because part of Rayleigh wave energy penetrates from one side to another of the horst directly. Moreover, there are less and less variations in frequency spectrum and finally reach a stabilization. In addition, the numerical results also display that the local depressed topography affects the propagation of high-frequency Rayleigh-waves more obviously than the local uplifted topography does.

Furthermore, local topography strongly influences the character of Rayleigh-wave dispersion. The energy concentration on the dispersion energy images may be distorted, due to the effect of the local topography. Egregious error may be introduced in picking the dispersion curve by the conventional energy tracing method, when the receivers are not located in a same elevation and no static correction is applied for an MASW survey. Finally, it leads to an incorrect explanation of earth model by inverting such dispersion curves.

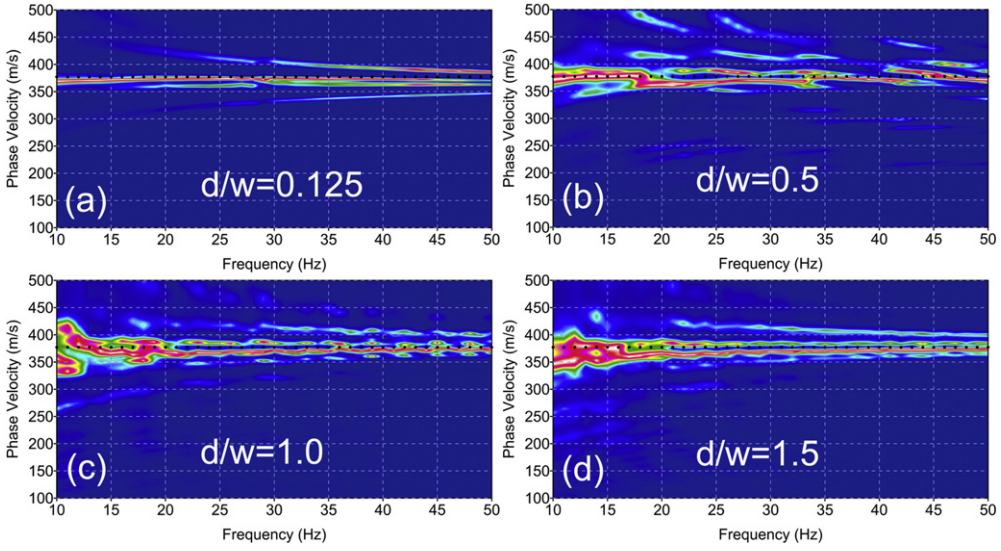

Fig. 17. The dispersion energy images of Rayleigh waves in elastic half-space model with depressed topographic free surface. The energy images are generated by the HRLRT method (Luo et al., 2008). The black dots denote the analytical dispersion curves of Rayleigh waves in elastic homogeneous half-space model, which are calculated by the Knopoff method (Schwab and Knopoff, 1972). Figures (a) to (d) are the dispersion energy images of Rayleigh waves in depressed topographic model with the steepness of d/w = 0.125, d/w = 0.5, d/w = 1.0, and d/w = 1.5, respectively.

Acknowledgments

This work is supported by the China Postdoctoral Science Foundation, under Grant No. 2013M542087, and by the Open Foundation of Hubei Subsurface Multi-scale Imaging Key Lab (SMIL), China University of Geosciences (Wuhan), under Grant No. SMIL-2014-08. The first author appreciates the Associate Professor Chi-Chia Tang of China University of Geoscience (Wuhan) for reading, commenting on the manuscript and helping to improve the language. We also thank the editor and the reviewer Giancarlo Dal Moro and another anonymous reviewer for their constructive criticism.

Appendix A. Supplementary data

Supplementary data to this article can be found online at http://dx.doi.org/10.1016/j.jappgeo.2015.02.028.

References

Bouchon, M., Schultz, C.A., Toksoz, M.N., 1996. Effect of three-dimensional topography on seismic motion. J. Geophys. Res. 101 (B3), 5835–5846.
Cao, M., Moreno, C., Quintelal, P., 2007. Simulation of Rayleigh waves in cracked plates. Math. Methods Appl. Sci. 30, 15–42.
Craig, R.F., 1992. Soil Mechanics. 5th ed. Chapman & Hall, New York.
deBremaecker, J.C., 1958. Transmission and reflection of Rayleigh waves at corners. Geophysics 23, 253–266.
Fujii, K., Takeuchi, S., Okano, Y., Nakano, M., 1984. Rayleigh wave scattering at various wedge corners. Bull. Seismol. Soc. Am. 74, 41–60.
Fuyuki, M., Matsumoto, Y., 1980. Finite difference analysis of Rayleigh wave scattering at a trench. Bull. Seismol. Soc. Am. 70, 2051–2069.
Hévin, G., Abraham, O., Pedersen, H.A., Campillo, M., 1998. Characterization of surface cracks with Rayleigh waves: a numerical model. Nondestruct. Test. Eval. Int. 31 (4), 289–297.
Hudson, J.A., Knopoff, L., 1964. Transmission and reflection of surface waves at a corner. J. Geophys. Res. 69, 281–289.
Imai, T., Tonouchi, K., 1982. Correlation of N-value with S-wave velocity. Proceedings of the Second European Symposium on Penetration Testing, pp. 67–72.
Kawase, H., 1988. Time-domain response of a semicircle canyon for incident SV, P, and Rayleigh waves calculated by the discrete wave-number boundary element method. Bull. Seismol. Soc. Am. 78, 1415–1437.
Knopoff, L., Gangi, A.F., 1960. Transmission and reflection of Rayleigh waves by wedges. Geophysics 25, 1203–1214.
Luo, Y., Xia, J., Miller, R.D., Xu, Y., Liu, J., Liu, Q., 2008. Rayleigh-wave dispersive energy imaging using a high-resolution linear Radon transform. Pure Appl. Geophys. 165, 903–922.
Mal, A.K., Knopoff, L., 1965. Transmission of Rayleigh waves past a step changes in elevation. Bull. Seismol. Soc. Am. 55, 319–334.
Mal, A.K., Knopoff, L., 1966. Transmission of Rayleigh waves at corner. Bull. Seismol. Soc. Am. 56, 455–466.
Mittet, R., Arntsen, B., 2000. General source and receiver positions in coarse-grid finite-difference schemes. J. Seism. Explor. 4, 5–16.
Nasseri-Moghaddam, A., Cascante, G., Phillips, C., Hutchinson, D.J., 2007. Effects of underground cavities on Rayleigh waves—field and numerical experiments. Soil Dyn. Earthq. Eng. 27, 300–313.
Robertsson, J.O., 1996. A numerical free-surface condition for elastic/viscoelastic finite-difference modeling in the presence of topography. Geophysics 61 (6), 1921–1934.
Sánchez-Sesma, F.J., Campillo, M., 1991. Diffraction of P, SV, and Rayleigh waves by topographic features: a boundary integral formulation. Bull. Seismol. Soc. Am. 81, 2234–2253.
Schwab, F.A., Knopoff, L., 1972. Fast surface wave and free mode computations. In: Bolt, B.A. (Ed.), Methods in Computational Physics. Academic Press, pp. 87–180.
Snieder, R., 1986. The influence of topography on the propagation and scattering of surface waves. Phys. Earth Planet. Inter. 44, 226–241.
Wang, L., Luo, Y., Xu, Y., 2012. Numerical investigation of Rayleigh-wave propagation on topography surface. J. Appl. Geophys. 86, 88–97.
Wong, H.L., 1982. Effect of surface topography on the diffraction of P, SV, and Rayleigh waves. Bull. Seismol. Soc. Am. 72 (4), 1167–1183.
Xia, J., Miller, R.D., Park, C.B., 1999. Estimation of near-surface shear-wave velocity by inversion of Rayleigh waves. Geophysics 64, 691–700.
Xia, J., Miller, R.D., Park, C.B., Hunter, J.A., Harris, J.B., Ivanov, J., 2002. Comparing shear-wave velocity profiles from multichannel analysis of surface wave with borehole measurements. Soil Dyn. Earthq. Eng. 22 (3), 181–190.
Xu, Y., Xia, J., Miller, R.D., 2007. Numerical investigation of implementation of air–earth boundary by acoustic–elastic boundary approach. Geophysics 72 (5), 147–153.
Zeng, C., Xia, J., Miller, R.D., Tsoflias, G.P., 2012a. An improved vacuum formulation for 2D finite-difference modeling of Rayleigh waves including surface topography and internal discontinuities. Geophysics 77 (1), 1–9.
Zeng, C., Xia, J., Miller, R.D., Tsoflias, G.P., Wang, Z., 2012b. Numerical investigation of MASW application in presence of surface topography. J. Appl. Geophys. 84, 52–60.
Zhang, J., Liu, T., 2000. Numerical simulation of elastic wave propagation in anisotropic media. Acta Mech. Solida Sin. 13 (1), 50–59.
Zhao, D., 1991. Tomographic Study of Seismic Velocity Structure in the Japan Islands. Tohoku University, Sendia.
Zhou, H., Chen, X., 2007. A study on the effect of depressed topography on Rayleigh surface wave. Chin. J. Geophys. 50 (4), 1018–1025.